ELSEVIER

Journal of Nuclear Materials 318 (2003) 38–55

journal of nuclear materials

www.elsevier.com/locate/jnucmat

R&D of A MW-class solid-target for a spallation neutron source

Masayoshi Kawai [a,*], Michihiro Furusaka [a], Kenji Kikuchi [b], Hiroaki Kurishita [c], Ryuzo Watanabe [d], Jing-Feng Li [d], Katsuhisa Sugimoto [d], Tsutomu Yamamura [d], Yutaka Hiraoka [e], Katsunori Abe [d], Akira Hasegawa [d], Masatoshi Yoshiie [f], Hiroyuki Takenaka [g], Katsuichiro Mishima [f], Yoshiaki Kiyanagi [h], Tetsuo Tanabe [i], Naoaki Yoshida [j], Tadashi Igarashi [k]

[a] *High Energy Accelerator Research Organization, Tsukuba-shi, Ibaraki-ken 305-0801, Japan*
[b] *Japan Atomic Energy Research Institute, Tokai-mura, Ibaraki-ken 319-1195, Japan*
[c] *Institute for Materials Research, Tohoku University, Oarai-machi, Ibaraki-ken 311-1313, Japan*
[d] *Graduate School of Engineering, Tohoku University, Sendai-shi, Miyagi-ken 980-8579, Japan*
[e] *Department of Applied Physics, Okayama University of Science, Okayama-shi 700-0005, Japan*
[f] *Research Reactor Institute, Kyoto University, Kumatori-cho, Osaka-fu 590-0494, Japan*
[g] *Department of Mechanical Engineering, Kobe University, Nada-ku, Kobe-shi 657-0013, Japan*
[h] *Graduate School of Engineering, Hokkaido University, Kita-ku, Sapporo-shi 060-8603, Japan*
[i] *Center for Integrated Research in Science and Engineering, Nagoya University, Nagoya-shi 464-0814, Japan*
[j] *Research Institute for Applied Mechanics, Kyushu University, Kasuga-shi, Fukuoka-ken 816-0811, Japan*
[k] *Osaka Prefecture University, Sakai-shi, Osaka-fu 599-8231, Japan*

Abstract

R&D for a MW-class solid target composed of tungsten was undertaken to produce a pulsed intense neutron source for a future neutron scattering-facility. In order to solve the corrosion of tungsten, tungsten target blocks were clad with tantalum by means of HIP'ing, brazing and electrolytic coating in a molten salt bath. The applicability of the HIP'ing method was tested through fabricating target blocks for KENS (spallation neutron source at KEK). A further investigation to certify the optimum HIP conditions was made with the small punch test method. The results showed that the optimum temperature was 1500 °C at which the W/Ta interface gave the strongest fracture strength. In the case of the block with a hole for thermocouple, it was found that the fabrication preciseness of a straight hole and a tantalum sheath influenced the results. The development of a tungsten stainless-steel alloy was tried to produce a bare tungsten target, using techniques in powder metallurgy. Corrosion tests for various tungsten alloys were made while varying the water temperature and velocity. The mass loss of tungsten in very slow water at 180 °C was as low as 0.022 mg/y, but increased remarkably with water velocity. Simulation experiments for radiation damage to supplement the STIP-III experiments were made to investigate material hardening by hydrogen and helium, and microstructures irradiated by electrons. Both experiments showed consistent results on the order of the dislocation numbers and irradiation hardness among the different tungsten materials. Thermal-hydraulic designs were made for two types of solid target system of tungsten: slab and rod geometry as a function of the proton beam power. The neutronic performance of a solid target system was compared with that of mercury target based on Monte Carlo calculations by using the MCNP code.

* Corresponding author. Tel.:+81-298 64 5637; fax:+81-298 64 3202.
E-mail address: masayoshi.kawai@kek.jp (M. Kawai).

0022-3115/03/$ - see front matter © 2003 Elsevier Science B.V. All rights reserved.
doi:10.1016/S0022-3115(03)00114-4

1. Introduction

We performed R&D work to determine and develop the optimum material for a long-lived and high-neutron-yield solid target for future MW-class spallation neutron sources for material science. Tungsten has many favorable properties as the solid target of a spallation neutron source. It has been used for high heat flux components and high-density structural materials under a radiation environment. High-density means high neutron yields. Accordingly, the tungsten is/was used for a spallation neutron target at some facilities, such as KENS [1] and LANSCE [2]. In the APT project [3], tungsten was selected for the target and elaborately studied at LANL. However, it was pointed out that tungsten has poor corrosion resistance against water coolants due to the formation of a ragged tungsten hydroxide [4], and intense susceptibility to radiation embrittlement [5]. One approach to avoid the former problem is to clad tungsten with a corrosion-resistant material, such as titanium, stainless steel, Zircaloy, niobium, tantalum or gold. The other approach to make an alloying metal or high-purity metal to solve problems. The key issue to strengthen the resistance against radiation damage is to improve the low-temperature embrittlement, recrystallization embrittlement and radiation embrittlement. Some investigations to achieve simultaneous improvements in these embrittlements were performed by Kurishita et al. [6] to develop tungsten alloys with microstructures of fine grains and finely dispersed particles of transition metal carbide using mechanical alloying (MA) and sintering techniques.

Accordingly, our main issue is to develop a fabrication method to solve the corrosion problem. Three kinds of methods to clad tungsten with tantalum were investigated: HIP (hot isostatic press) [7,8], brazing and electrolytic coating in a molten salt bath. Stainless-steel-bonded tungsten alloy was newly developed as a latter approach. A corrosion test was made for several kinds of tungsten alloys, such as high-purity tungsten W–Re alloy and MA-fabricated tungsten alloy by changing the aqueous conditions, such as the water flow velocity and the temperature. As for irradiation effects, ion and electron bombardment tests were made to obtain data to supplement that from the STIP-III experiments [9] at PSI.

As a sample problem, thermal-hydraulic designs were made for both slab and rod type targets as a function of the proton beam power up to 5 MW. The neutronics performance of typical solid targets with 1 MW was compared with that of a mercury target.

2. Methods for manufacturing of a tantalum-clad tungsten target

As for the cladding material, stainless steel, inconel and Zircaloy are the most popular, and experience has been gained by using it as a clad for the fuel rods of nuclear reactors. This has led to a high dose rate of several tens of dpa. However, the users of neutron scattering facilities hope that the neutron yield will be as high as possible. Tantalum is promising because its density is the highest among the candidate materials, except for gold. In addition, it was found that tantalum specimens which were taken off from the tantalum target bombarded by a 800 MeV proton beam and secondary neutrons up to a dose of 13 dpa at the ISIS facility of Rutherford Appleton did not lose their ductility [10], while previous irradiation experiments showed that tantalum increased in hardness upon experiencing neutron irradiation, like tungsten [5]. This result for tantalum, and the experience of using tungsten target and the 800 MeV proton irradiation experiments for the APT and ADTF projects at LANSCE [11,12] give us hope for a long-life solid target with good performance by manufacturing a tungsten block and tantalum clad. The key of clad is not to have any pin holes in the tantalum and to bond both materials perfectly so as to achieve a good thermal conduction to remove any heat deposited by a high-energy proton beam from target. Electrolytic coating, thermal spraying with a plasma, and similar methods may be useful to form a thin layer on a large plate, but some of these techniques have difficulties of coating around a hole or peeling off from the target under proton-beam irradiation. We investigated the applicability of three methods: HIP'ing, brazing and electrolytic coating in a molten salt bath. The former two methods are very popular for many kinds of structural materials, but very rare to bonding tungsten and tantalum. The last method is a new, and the first trial is noted in this paper.

2.1. HIP'ing method

2.1.1. Fabrication of a tantalum-clad tungsten block

ISIS developed [13] a tantalum-clad tungsten target block by means of the HIP'ing at 1400 °C and a high pressure of 1450 MPa. However, such conditions are not easily attained with an ordinary HIP. In previous work [7], we found the optimum HIP conditions with respect to a temperature of 1500 °C, pressure of 200 MPa and impurity gas control using high-purity argon gas (5N or 6N) and gas-getter materials of zirconium foils and tantalum plates. We then applied it to the fabrication of a real target block for KENS, and succeeded to produce HIP'ing blocks. However, the method was not perfect for a block with a hole.

After that, we investigated the origins of leading to a HIP defect and the methods to remove them. At first, we found a small crack in a hole cut in an intermediate part of an unsuccessful target block, where an ultrasonic pattern showed an obvious defect between the tungsten and tantalum [8]. The crack penetrated from inside of a

sheath of 80 μm thickness to the outside, while it became closed near the outside surface upon decreasing the temperature and pressure in the HIP procedure.

We then measured the Vickers micro hardness of the tantalum sheath and tungsten near the crack. The measurement of hardness was made after polishing a cross-section by about several micrometers. Fig. 1 shows the hardness results as a function of the distance from the tungsten–tantalum boundary. From this figure, we can see a fairly wide gap of several tens of micrometers between the tungsten and tantalum. The gap i.e. clearance, seems to be too large compared to the design values of a tungsten hole diameter of $3.2+0.03$–0 mm and an outer diameter of tantalum sheath $3.2+0$–0.03 mm and the curvature of tungsten surface is not so smooth. This means that there might have been some problems in fabricating the block and/or tantalum sheath, as shown by the fact that a hole which had been made in tungsten on a trial piece tapered from 3.16 mm at the entrance to 3.06 mm at the bottom.

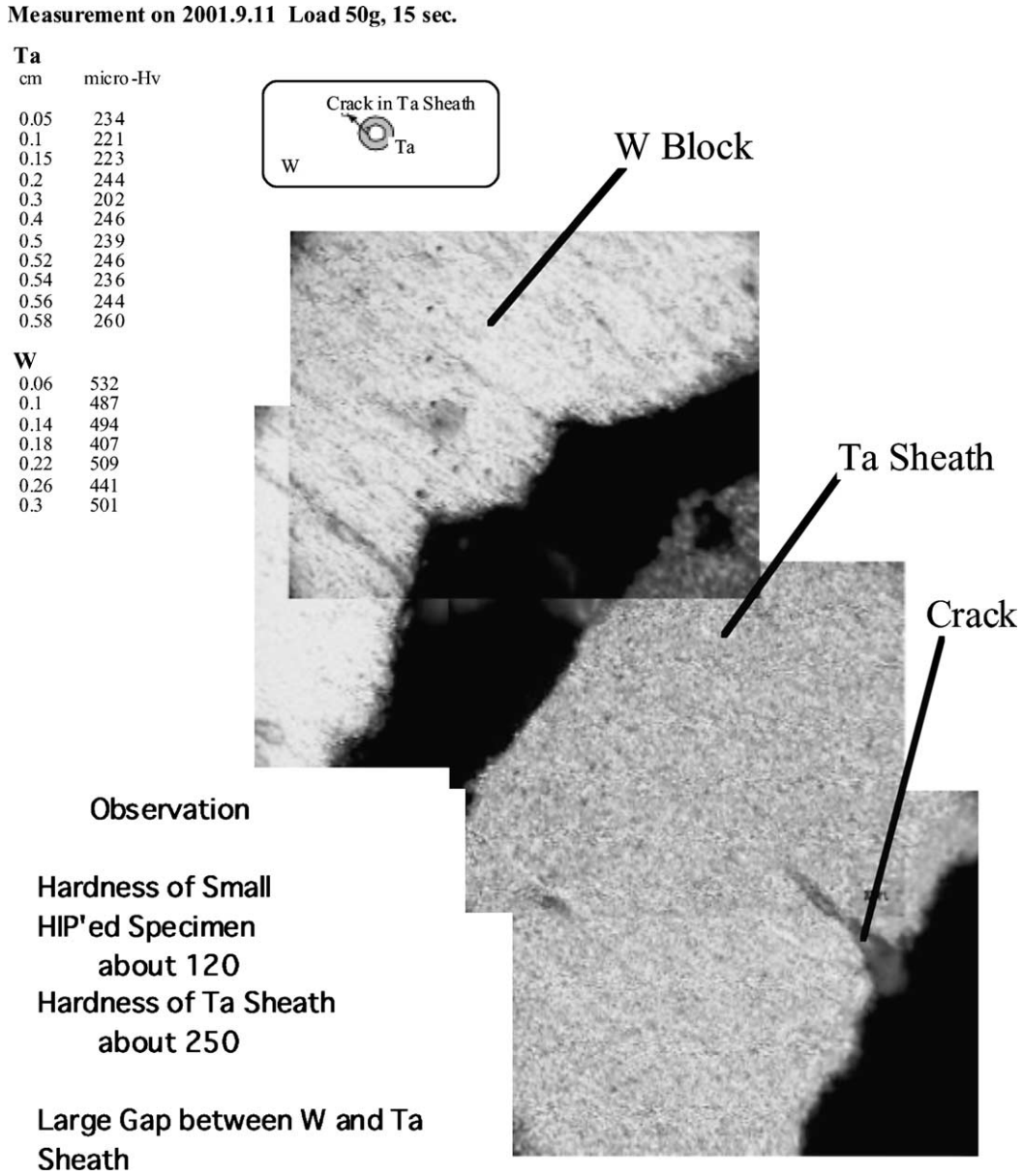

Fig. 1. Cross-section of a part of a tungsten block and a tantalum sheath with a crack induced by HIP and their micro-Vickes hardness.

The measured values of the hardness of the tantalum sheath were about twice that of ordinary processed tantalum, while those of tungsten were almost the same as that of ordinary tungsten. Impurity gas and mechanical hardening did not seem probable as the reason to harden the tantalum sheath. The latter has bee denied because experiments to anneal the tantalum sheath up to 800 and 1400 °C did not show a very large change in the hardness. On the other hand, a chemical analysis was made for a tungsten layer around a test hole that was cleaned up using acid and an organic solvent, as was done for the actual target block. It did not show that the contents of the impurity gas elements, such as nitrogen, oxygen and carbon, were under the detectable level. An analysis for the tantalum sheath was not made because we could not remove the sheath from the tungsten block. Accordingly, the obvious conclusion for what process hardened the sheath has not been determined so far. In any case, we are confident that the key technology for HIP'ing a block with a hole is to make a straight hole in the tungsten with very high accuracy and without any fine crack, and to shape a tantalum sheath without hardening.

We tried to fabricate a tungsten block with a hole, again. The hole was shaped in the tungsten block with five steps: electric discharge machinery (EDM) (2.9 mm in diameter), plunge EDM and machining with a high-strength drill and reamers. The value of the initial diameter by the EDM method was determined as follows. We observed a test hole started from 3.0 mm diameter to the desired value of 3.22 mm with an optical microscope. Fig. 2 shows many micro-cracks within several tens of micrometers from the surface in the cross-section of the hole. Their depths were measured with a laser microscope to be about 30 μm in maximum. The micro-cracks were formed during the initial EDM process and also possibly include gas impurities. On the other hand, tungsten is too hard to machine with a high-strength drill and reamer. It was thus concluded to cut the hole with EDM and to remove most of the micro-cracks layer, i.e, removed layer thickness is 160 μm after the initial EDM process.

Finally, we fabricated a tungsten block and obtained a straight hole of 3.22 mm in diameter within an accuracy of several tens of micrometers. The block was coated with tantalum and equipped with a tantalum sheath by blowing out air by argon gas. They were temporarily bonded at several places by TIG welding and perfectly sealed by electron beam welding in an environment under vacuum conditions. The HIP'ing was made with the optimum condition, which is described in detail in Ref. [7]. The HIP'ed block was checked by ultrasonic diagnostics. They did not show any abnormal pattern.

2.1.2. Evaluation of bonding interface

The bonding integrity of the interface between the tantalum clad and the tungsten block is of first concern for a spallation target because bonding defects, if any, would result in peeling off the corrosion-resistant surface layer, and thus leading to shortening of the target life. Raising the HIP'ing temperature is effective to obtain a high-strength interface. However, the recrystallization and grain coarsening of tungsten and tantalum may be

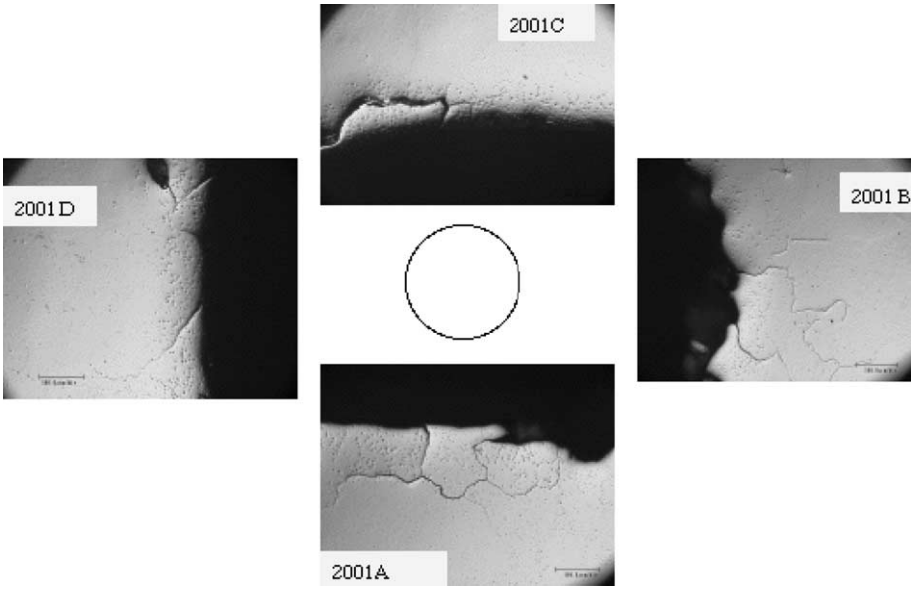

Fig. 2. Microscopic graph of the cross-section of a tungsten hole shaped with EDM.

enhanced simultaneously during HIP at high temperature, which would result in a decrease in the fracture toughness of the target. It is therefore necessary to optimize the HIP cladding temperature. In the present study, the bonding strength of the W–Ta interface was evaluated using the small punch test (SP test) [14,15], and the diffusion thickness across the interface was measured by the electron probe micro-analysis (EPMA) [16].

An SP test was made with disk-shaped specimens (see Fig. 3). The stress is defined as follows (but strictly only for the onset of loading when the plain contact is present between the punch and the specimen):

$$\sigma_{\max} = \frac{3P}{2\pi t^2}(1+v)\left[1 - \frac{1-v^2}{4}\cdot\frac{b^2}{a} + (1+v)\ln\frac{a}{b}\right], \qquad (1)$$

where $\sigma_{\max}$ is the nominal maximum fracture stress, P is the load at the fracture, t is the specimen thickness, v is Poisson's ratio, a and b are the radii of the punch and the loading area, respectively.

The SP samples were prepared by the following procedures. First, tungsten and tantalum billets with a semicircle cross-section (radius = 5 mm) were cut from the same materials as that of the target. The rectangular longitudinal cross-section was polished to the same finish as the tantalum can and tungsten block for the targets. The polished sections of both billets were put together and inserted into a tantalum tube (inner diameter = 10 mm, thickness = 1 mm). The tube was vacuum-sealed by electron-beam welding, and HIP'ed under the same conditions as in the HIP cladding. Finally, the HIP'ed sample was sliced into thin-disk specimens, one half of which were tungsten and the other half were tantalum. After polishing the disk surface, the specimens were subjected to SP testing, in which a load was applied to the specimen center, i.e., at the center of the bonded interface. In load deflection curves, a load drop was observed before the eventual fracture for all of the specimens. We defined the SP load at the load-drop point as a fracture load. Fig. 4 shows the fracture load and the strength calculated by Eq. (1) as a function of the HIP'ing temperature. The fracture strength was the maximum at 1500 °C.

By SEM observation, it was found that such a load drop corresponded to crack initiation. Regardless of the HIP'ing temperature, a crack was formed and propagated within tungsten. This observation suggests that the interface formed under the present HIP'ing conditions was well bonded, with a bonding strength at least higher than the fracture strength of the tungsten block. However, when the HIP'ing temperature exceeded 1500 °C, the load for the crack initiation, as well as the fracture strength, decreased due to recrystallization in the tungsten. Therefore, the optimal HIP'ing temperature was

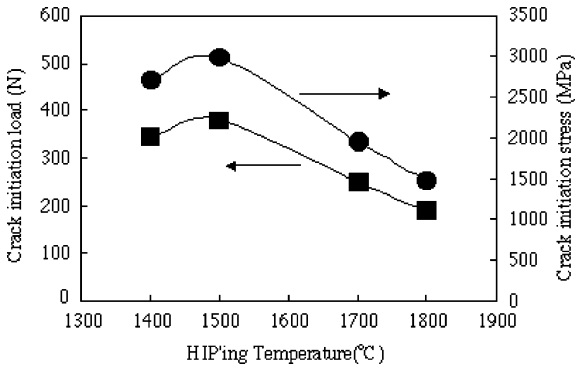

Fig. 4. Crack initiation load measured in small punch test for the bonded specimens of tungsten and tantalum, and the crack initiation stress estimated with Eq. (1).

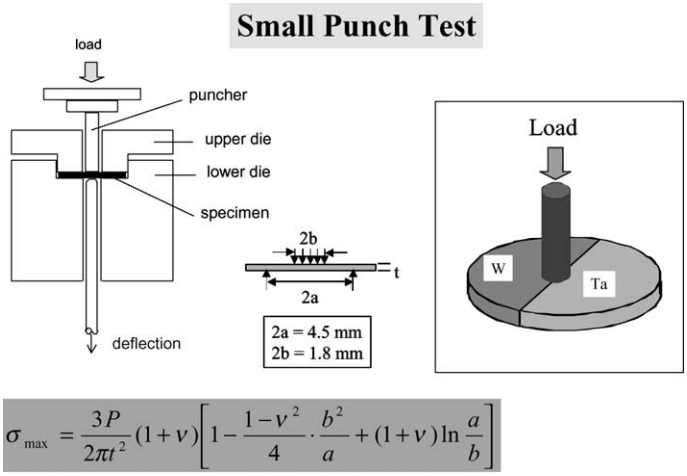

Fig. 3. Schematic illustration of a small punch set-up and the loading condition.

determined to be 1500 °C. The diffusion thickness formed at this temperature was measured by EMPA to be 3.5 μm [7].

2.2. Brazing method

The braze method for cladding a tungsten block was tried at first by using platinum, because tantalum and platinum are both favorable from the viewpoints of the neutron yield. Its brazing was successful, but its joint strength was much lower than the fracture strength of bulk tungsten (610–835 MPa). Then, brazing was performed by using titanium.

A set of samples, as schematically drawn in Fig. 5 was heated up to 1680 °C and held for 120 s at this temperature, followed by furnace-cooling. The brazing atmosphere was vacuum of $< 1 \times 10^{-5}$ Torr. The joints using titanium brazing between tungsten and tantalum were designated as 'W/Ti/Ta'. A hardness test for a small specimen was performed at room temperature with 50 g of load and a 15 s holding time after an EPMA analysis. Three-point bend tests were also made to a rectangular specimen. Careful attention was paid to place the brazed layer almost in the center of the specimen and normal to the specimen axis. After each test, the fracture surface was observed by using SEM and the fracture mode was examined.

2.2.1. Result of an EPMA analysis

The contents of Ta and W in the brazing layer were higher in case of W/Ti/Ta than W/Pt/Ta. The tantalum contents in a titanium layer of 120 μm remained at a relatively high level, and then decreased slowly with the distance from the tantalum surface up to 115 μm, i.e. 5 μm from the tungsten surface, while tungsten decreased steeply within 5 μm from the tungsten surface and slowly to zero at the tantalum surface. In the case of platinum brazing, tantalum and tungsten diffused several tens of micrometers into the platinium layer of 90 μm.

2.2.2. Hardness

Fig. 6 shows the distribution of hardness in the brazed layer and its vicinity of the joints. The hardness in the brazed layer of the joint Ta/Ti/W ranged between 250 and 400 Hv. The spatial change of hardness at the interface Ta/Ti was slow, while the hardness at Ti/W interface showed small peak. As for brazing with platinum, the hardness of brazing layer was about 130 Hv, approximately as low as that of bulk Ta, and showed a very high peak (about 830 Hv) at the Ta/Pt interface. The hardness at this interface decreased by annealing at 1500 °C after brazing.

2.2.3. Bend test

The fracture strength was 500–570 MPa for the Ta/Ti/W joint and 200–370 MPa for Ta/Pt/W. The fracture site of the Ta/Ti/W joint was along the Ti/W interface, while that of the Ta/Pt/W joint was along the Ta/Pt interface.

As a whole, the titanium gave a better result than the platinum as shown by the hardness without a large change, and by the large fracture strength above 500 MPa.

2.3. Electrolytic tantalum coating of a tungsten substrate in molten salt bath

In this study, a dense and compact coating of tantalum on nickel was pursued to attain a tantalum coating on a tungsten substrate mediated by a thin nickel layer by using a molten salt bath. It has been known that Ni and W form an intermetallic compound,

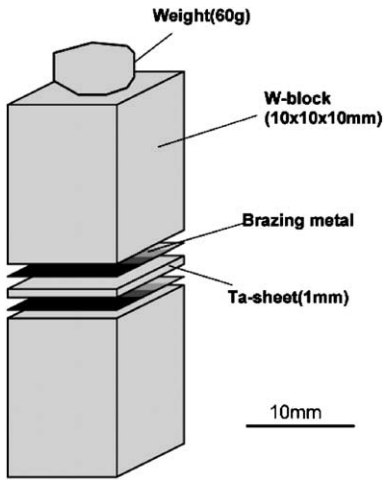

Fig. 5. Schematic of the brazing procedure.

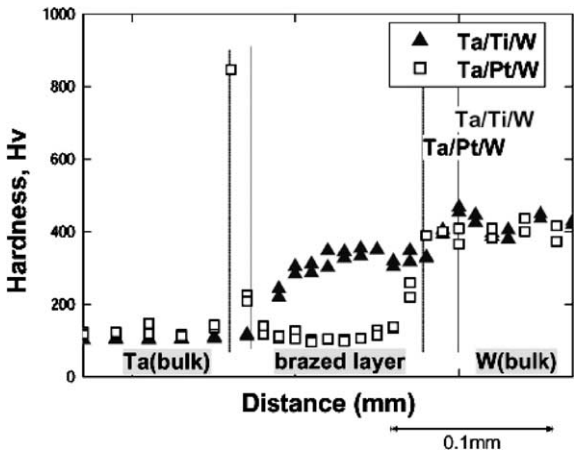

Fig. 6. Hardness distribution across the brazed layer in the joints, Ta/Ti/W and Ta/Pt/W.

WNi_4, which might work as another mediating layer between W and Ni layers. Therefore, it is expected that corrosion-resistant tantalum coating of tungsten would be attained through The Ta/thin Ni layer/W scheme shown in Fig. 7. As a first step, the deposition of a dense and compact coating of tantalum on nickel was tried in this study.

2.3.1. Experimental

The electrolyte consisted of 55%LiF–35%NaF–10%CaF_2 in which 1% K_2TaF_7 was added (percentage is given in mole percent). The cell consisted of a graphite crucible. A nickel rod was used as a quasi-reference electrode and a graphite rod was used as a counter electrode. The electro-deposition was carried out at 700 °C under an argon atmosphere.

2.3.2. Results and discussion

A cross-sectional view of a nickel wire (1-mm diameter) on which tantalum had been coated revealed that a continuous and rather smooth deposition was attained, as shown in Fig. 8. The experiment was repeated several times, and similar results were obtained. A cross-sectional view at a higher magnification is shown in Fig. 9. Tantalum is present in two layers. The nickel content appears to be negligible in the upper layer. However, the lower layer contains a significant concentration of nickel. This layer seems to be formed as the result of the diffusion of tantalum into the nickel substrate at high temperature. The X-ray spectrum obtained from the upper layer indicated that this layer did not contain any appreciable nickel. The analysis showed the tantalum content to be close 100%. Hence, nickel did not diffuse into the tantalum coating.

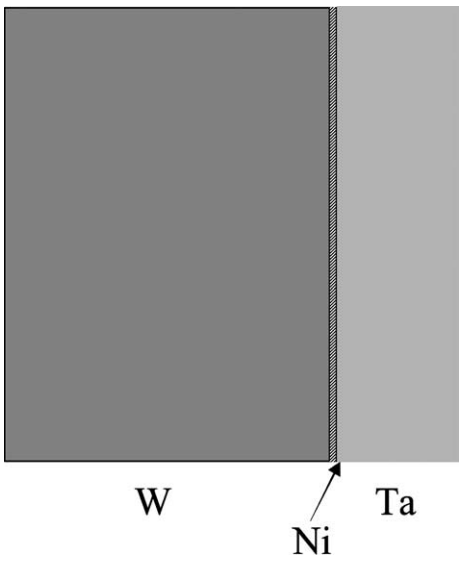

Fig. 7. Schematic diagram of the proposed coating of tantalum on a tungsten target.

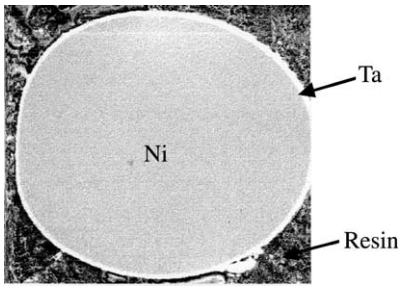

Fig. 8. Cross-sectional view of a 1-mm nickel wire electroplated with tantalum. The coating covers the alloy surface completely.

The present results can be summarized as follows: The plating of pure tantalum on nickel was performed by molten salt electro-deposition. The coating was dense and compact. Based on the present results, it is expected that corrosion-resistant tantalum coating of tungsten could be attained by a simple and economic electrolytic coating technique using a molten salt bath.

2.4. Development of tungsten–stainless-steel alloy

The corrosion of a tungsten heavy alloy (97W–Ni–Cu–Fe) under a wet condition was remarkably improved by the addition of a small amount of chromium [4]. It seemed that the chromium addition improved the corrosion resistance of the binder phase. In the present work, a 304-type stainless steel was used as a corrosion-resistant binder [16]. Here is the brief description of the development of a tungsten–stainless-steel alloy.

2.4.1. Specimen preparation

Tungsten powders of 5 and 9 μm in average size and a stainless-steel powder (SUS304L: 0.017C, 08Si, 0.1Mn, 0.025P, 0.005S, 18.2Cr, 10.8Ni, Fe(bal)) of 8.2 μm were used as the starting materials. They were mixed in wt% of 93 and 97W by wet milling. The dried and disintegrated powder was die-compacted at 150 MPa to a cylindrical form of 10 mm in diameter and 15 mm in height, and subsequently CIP'ed (cold isostatic pressed) at 200 MPa to eliminate any density inhomogeneity generated by die wall friction. The densification behavior during vacuum-sintering and HIP'ing was investigated as a function of the sintering temperature and holding time: (1) Vacuum sintering was conducted in a temperature range of 1350–1550 °C above the melting point of the stainless-steel phase, and a time interval of 5 min–5 h in a tungsten-mesh heater furnace using a boron nitride crucible as a sample holder. (2) The sintered compacts were HIP'ed to eliminate any residual pores at 200 MPa and 1500 °C. (3) Some samples were liquid-phase-sintered in hydrogen, or directly HIP'ed

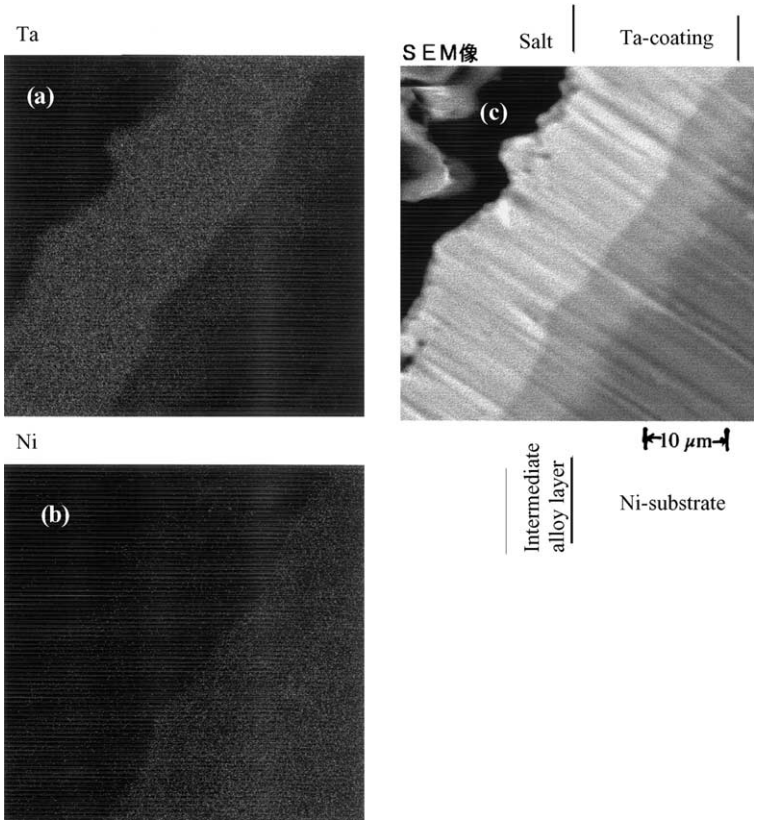

Fig. 9. Typical characteristic X-ray maps of (a) tantalum, (b) nickel and (c) taken from a nickel-plated section with the corresponding SEM image. As shown in the figures, the Ni layer is connected to Ta through an intermediate alloy layer. This fact indicates the excellent adherence of a Ta coating to a Ni layer.

below the melting point of the stainless steel (1400–1450 °C) to find any microstructure variations.

2.4.2. Microstructure

Three zones having different microstructures were observed in a micrograph of the cross-section of the sample vacuum sintered 1 h at 1450 °C. They are a mono-phase surface layer, a dense intermediate layer and a porous core. The surface shell structure would have been formed by vaporization of the binder phase during liquid-phase sintering. Pore elimination in the center core is supposed to be suppressed by the formation of this dense shell structure. On the other hand, a homogeneously distributed heavy alloy structure was obtained by hydrogen sintering.

Fig. 10 shows typical microstructures of vacuum and hydrogen sintered samples that were HIP'ed at 1500 °C after sintering at 1450 °C. Both exhibit the typical heavy alloy-type microstructure. The photomicrograph of the vacuum-sintered sample was taken from the binder-depleted intermediate zone where small pores still remained mainly in the binder phase. On the other hand, in the binder phase of the hydrogen-sintered sample angular voids are seen to exist, which would be solidification blow holes formed during cooling from the sintering temperature. The relative densities of the HIP'ed samples approach to 100% as the temperature and isothermal holding time increased during liquid-phase sintering, but remained at about 98% because of residual pores. A density of 93%W–7%SUS alloy received sintering at 1500 °C was higher than that of 97%W–3%SUS alloy, while it was vice versa at low temperature.

A composition analysis by EPMA showed that W dissolved into the binder phase by 72 wt%, whereas iron and chromium in the binder phase were found to dissolve into the W phase by about 1% or less. Judging from the phase diagrams of W–Fe, W–Ni, and W–Cr, tungsten dissolution into the binder phase by several tens of wt% would not increase the melting point of the binder. Complete densification and a typical heavy alloy structure would require a sintering temperature higher than 1500 °C for this alloy.

2.4.3. Thermal and mechanical properties

The thermal conductivity of the present 93W alloy was measured by a laser flash method (Netzsch

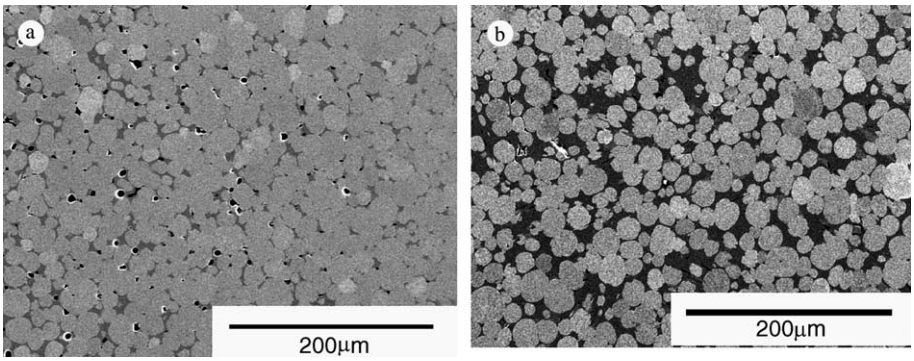

Fig. 10. Typical heavy alloy structures of the specimens HIP-treated for 3 h at 1500 °C after normal sintering. (a) Vacuum sintered for 1 h at 1450 °C, (b) hydrogen sintered for 1 h at 1450 °C.

LFA427), as shown in Fig. 11, along with the data for tungsten and stainless steel. The present alloy has lower thermal conductivity compared with that of the conventional alloy, and its temperature dependenceis rather similar to that of stainless steel, that is, the thermal conductivity increases with the temperature.

The strength and toughness of the present alloy was evaluated by a small punch test [14,15] with disk-shaped specimens. Fig. 12 shows the load–deflection curves for liquid-phase-sintered 93W–7stainless steel and solid-state consolidated alloys. The liquid-phase-sintered specimen exhibited a serrated deflection curve that indicates a multiple mode of crack propagation, whereas the solid-state consolidated specimen is seen to be brittle. The multiple-mode fracture observed in the liquid-phase sintered alloy would be preferable to alleviate radiation embrittlement.

In the present work, we could not obtain the heavy metal expected in the phase diagram and thermal conductivity, but the technique is considered to be worthwhile for powder metallurgy.

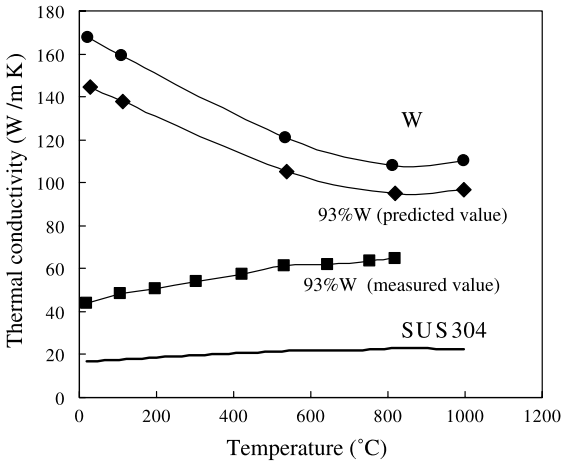

Fig. 11. Thermal conductivity of the present 93W–7stainless-steel alloy compared withthose of tungsten and stainless steel.

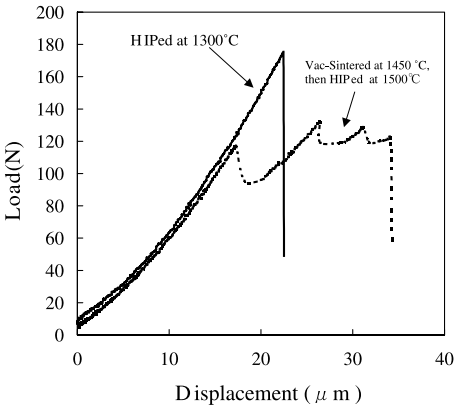

Fig. 12. Load–deflection curves for the liquid-phase-sintered 93W–7stainless steel and solid-state consolidated alloys.

3. Corrosion measurements on a tugsten

There are very few data available on the corrosion rates of tungsten in high-temperature water [17,18], and it is very valuable in spallation materials technology as well as in the development of fusion reactors. In the present work, two kinds of corrosion tests for available tungsten and its alloys together with the tungsten–stainless alloy described in Section 2.4 were made at Tohoku University. One was a basic experiment to reveal the corrosion resistance of W and its alloys for spallation targets in stagnant and high flow-rate water at 100 °C. The other was a corrosion-accelerated test at higher temperature. No irradiation was introduced to clarify the effect of the corrosion environment.

3.1. Test in aqueous solution at 100 °C

Polycrystalline W (99.99 mass%, PFW), high-purity polycrystalline W (99.999 mass%, 5N-W), super high-purity polycrystalline W made by CVD (99.9999 mass%, CVD-W), W-2 mass% Ta alloy (W–2Ta), W-5 mass% Re alloy (W–5Re), and 93 mass% W + 7 mass% SUS304 (Fe–18Cr–10Ni) sintered alloy (W–SUS) were used as specimens. In order to evaluate the corrosion resistances of the specimens, corrosion tests in boiling water at 100 °C under atmosphere, in pressurized water under 1.013 MPa H_2 at 100 and 180 °C, and in high flow-rate water saturated by H_2 at 100 °C were carried out. Before and after the corrosion tests, depth profiles of elements on the specimen surface were obtained by Auger electron spectroscopy (AES). The chemical states of elements on the surfaces were measured by X-ray photoelectron spectroscopy (XPS). The electrochemical characteristics of W and W alloys were analyzed using potentio-dynamic polarization curves measured in 1.0 kmol m^{-3} Na_2SO_4 of pH 2, 4.05, and 6.75 at 100 °C.

Typical results of the corrosion mass loss of the specimens in water are shown in Fig. 13. Fig. 13(a) shows that the corrosion mass loss decreased in the order W–SUS > W–5Re > 5N-W > PFW > W–2Ta > CVD-W. The corrosion mass loss at 100 °C in pressurized water decreased by several tens of percent compared with that in boiling water. In the case of CVD-W, the decrease of the corrosion loss was remarkable: the corrosion mass loss became below the analytical limits of 0.14×10^{-4} kg/m^2 at 100 °C and 0.16×10^{-4} kg/m^2 at 180 °C. The corrosion mass loss decreased in the order PFW > W–5Re > W–2Ta > 5N-W > CVD-W; that is, it decreased with increasing purity. In Fig. 13(b), the corrosion mass losses in stagnant and flowing water saturated by H^2 at 100 °C for 180 ks are shown as a function of the flow-rate. In flowing water, the corrosion mass loss sharply increased with increasing flow-rate. It also increased with increasing purity of the specimen as CVD-W > 5N-W > PFW.

From the results of the AES depth measurement, the thickness of the surface film after the corrosion test in stagnant water was less than a few nm. In the case of the test in flowing water, the film thickness on 5N-W was about 20 nm. From the results of the XPS measurement shown in Fig. 14, surface films after the corrosion tests in H_2-pressurized water were composed of WO_2, $WO_Y (2 < Y < 3)$, WO_3, and H_2WO_4.

The polarization curves of tungsten and tungsten alloys were taken in a 1.0 kmol m^{-3} Na_2SO_4 (pH 6.75) solution. The anodic polarization curves show the active dissolution of W from the corrosion potentials up to the diffusion limitation region. The cathodic polarization curves show small diffusion currents of the H^+ ions down to the active H_2 evolution region. The anodic polarization of W–SUS near to the corrosion potential was smallest among the specimens. However, the anodic and cathodic polarization curves were close to one another. The large limiting currents on the anodic polarization curves show that the films formed on the specimens are porous and poor in corrosion protection.

3.2. Corrosion-accelerated test

Corrosion-accelerated tests were made [19] in order to examine the corrosion resistance of refractory metals

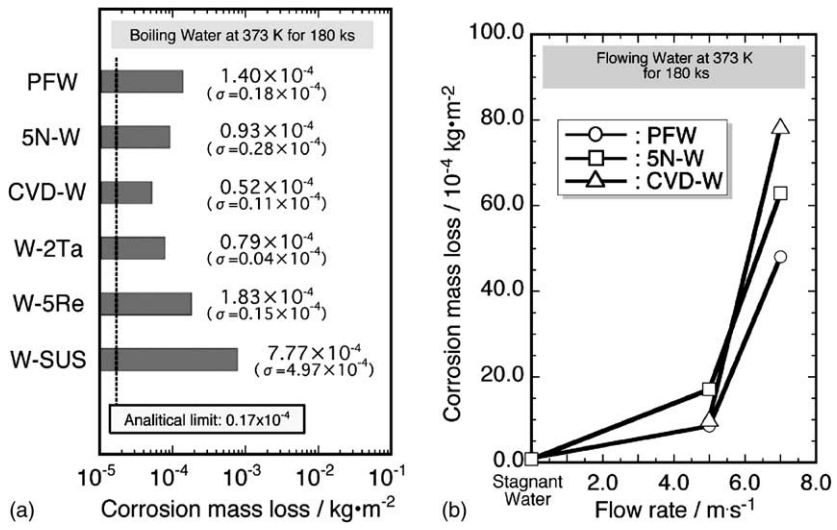

Fig. 13. Corrosion mass loss of W and W alloys (a) in boiling water and (b) in stagnant and flowing water saturated by H_2 at 373 K for 180 ks.

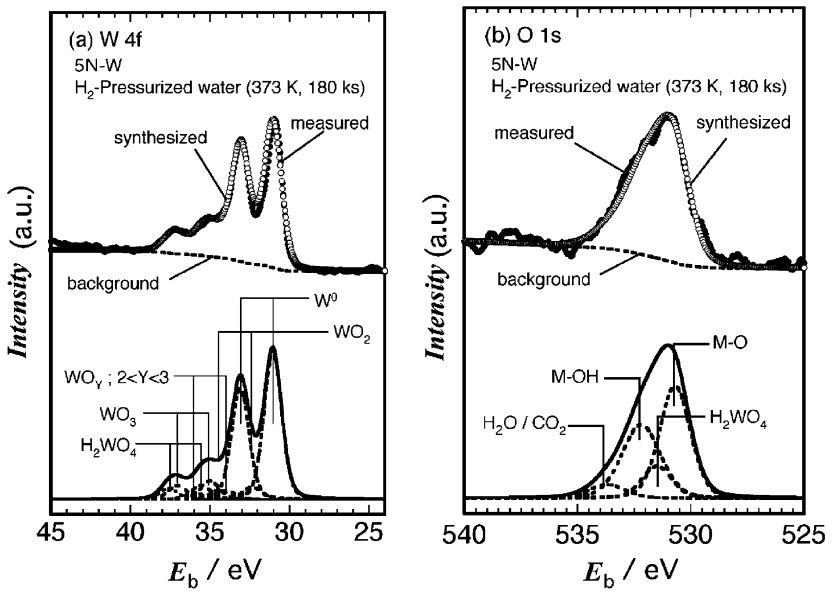

Fig. 14. Deconvoluted W 4f and O 1s XPS spectra of 5N-W after corrosion test in water pressurized under 1.013 MPa H_2 at 373 K for 180 ks.

in high-temperature water, 17 kinds of tungsten, in flowing water at a low flow-rate with a controlled dissolved oxygen content of 400 ppb and pH 6–7 at 180, 260 and 320 °C for 200 h. Before and after each test, measurements of the weight and X-ray diffraction (XRD) and observations of the surface appearance were performed.

Fig. 15 shows the weight gain and corrosion rate as a function of the test condition. It is obvious that in most cases the weight loss occurs and the magnitude of weight loss strongly depends on the test temperature and the material. In the case of commercial-grade pure tungsten (W-P), at 180 and 260 °C the weight loss remains almost constant, ~100 mg/dm^2, while at 320 °C it increases rapidly to ~900 mg/dm^2, which corresponds to 0.022 and 0.2 mm/y, respectively. The value of 0.022 mm/y belongs to class B (0.0125~0.125 mm/y: medium corrosion resistant and judged usable) and 0.2 mm/y to class C: (above 0.125 mm/y: poor corrosion resistant and judged unusable) [20]. Therefore, we can say that pure tungsten may be used in water with a dissolved oxygen content of 400 ppb and pH 6–7 at and below 260 °C, although data on the corrosion rate at much longer times than 200 h are required.

It can be seen from the figure that at 180 °C there is no significant difference in the weight loss between W-P and the other materials, except for CrN/W. At 260 °C only the heavy alloys (HM–7S, HM–7ST and HM185) show a significant increase in weight loss: one order larger than W-P, indicating that the heavy alloys cannot be used at 260 °C. At 320 °C, for most of tungsten the corrosion attack is promoted, with significant difference in corrosion rate between materials. The lowest corrosion-resistant material is W-(2–3)%Re alloy: ~7000 mg/dm^2 (~1.656 mm/y). It should be noted that CrN/W shows a small weight loss, ~20 mg/dm^2, which corresponds to ~0.004 mm/y, even at such a high temperature. This value belongs to class A (less than 0.0125 mm/y: good corrosion resistant).

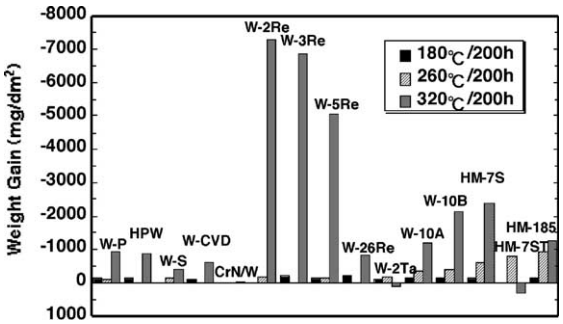

Fig. 15. Weight gain as a function of the testing temperature for tungsten.

The single crystal (W-S) showed less weight loss compared with W-P, and the coarse-grained W–10%Cu (W-10A) showed less weight loss than the fine-grained one (W-10B). This indicates that a detrimental effect of the grain boundaries promoting a corrosion attack occurred at 320 °C. It is also interesting to note that W–2Ta and HM–7ST show a change from weight loss at and below 260 °C to weight gain at 320 °C by forming corrosion product films that could be exfoliated.

Fig. 16 gives a typical example of XRD pattern taken from W-P tested at 320 °C. The large peaks of WO_3 and

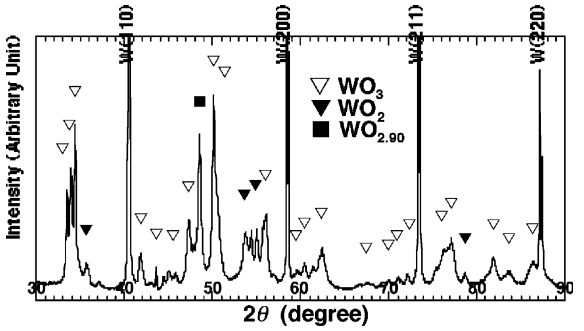

Fig. 16. X-ray diffraction pattern taken from an unalloyed tungsten polycrystal (W-P).

$WO_{2.9}$ and small peaks of WO_2 occur together with strong peaks of tungsten. Similar results were obtained for 320 °C-tested specimens of HP–W, W-S, CVD-W and W–5Re.

3.3. Summary

The results of two corrosion tests are summarized as follows:

(1) The corrosion mass loss of pure tungsten in water below 260 °C is low at a low flow-rate.
(2) The corrosion mass loss of W and W alloys in stagnant water decreases with increasing purity of the specimens.
(3) The trend that the corrosion mass loss of W alloys is larger than that of pure tungsten is prominent at high temperature, such as 320 °C.
(4) The addition of H_2 to water suppresses the corrosion of W and W alloys in water.
(5) The corrosion mass loss of W and W alloys in flowing water increases with increasing purity of the specimens.
(6) Surface films formed by the corrosion tests are composed of WO_2, $WO_Y(2 < Y < 3)$, WO_3, and H_2WO_4.
(7) The films formed in a neutral solution are thought to be porous and poor in corrosion protection.
(8) CrN/W has a quite strong resistance to corrosion.
(9) A low mass loss of pure W in stagnant water seems that a bare tungsten target will be promising, but an increase of mass loss with the water flow-rate should force ones to abandon the bare tungsten as a solid target for a MW class spallation neutron sources.

4. Irradiation damage in a solid tungsten target

Specimens of five kinds tungsten, gold and platinum alloy (90Pt–10Au) are being investigated in the STIP-III experiments together with structural materials. Additional irradiation experiments were performed to investigate the mechanism of radiation damage for tungsten using electron and ion accelerators.

4.1. Electron irradiation

High-voltage electron microscopy (HVEM) has the following advantages to study the irradiation damage of materials: the defect production rate is high and direct observation of defect evolution is possible. To study irradiation effects in tungsten, electron irradiation experiments using HVEM were performed for four types of tungsten specimens, and the formation behaviors of secondary defects were compared.

Three of them were sintered tungsten with a purity of 99.999% (5N-W), 99.99% (PF-W) and 99.95% (N-W). The highest purity of tungsten used in this experiment was 99.9999% (CVD-W) made by chemical vapor deposition. N-W was one available commercially. Irradiations and observations were made with a 3 MeV electron microscopy (Hitachi H-3000) of the Research Center for ultra-high voltage electron microscopy, Osaka University with an accelerating voltage of 2 MeV at temperatures of between room temperature and 600 °C. The irradiation time at each temperature was 180 s (~5 dpa).

The formation and growth of interstitial-type dislocation loops were observed. Their number density was high at lower temperatures, and almost no loops were formed above 500 °C. The number density of interstitial type dislocation loops was in the order of N-W > CVD-W > PF-W > 5N-W, as shown in Fig. 17. Except for CVD-W, it depended on the purity. The density of the loops was lower in higher purity tungsten. In the case of CVD-W, though the purity was high; a high density of interstitial type dislocation loops was formed. At lower

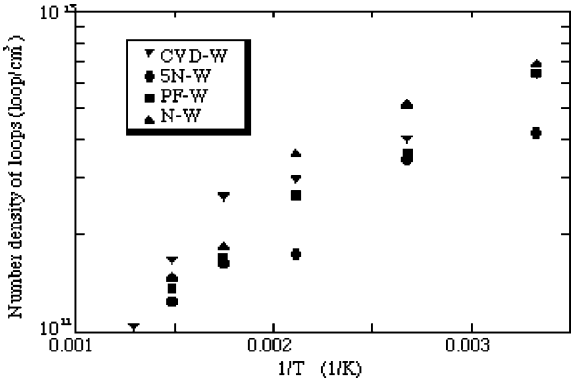

Fig. 17. Number density of interstitial type dislocation loops in tungsten formed by electron with 2 MeV as a function of irradiated temperature.

temperatures, many interstitial-type dislocation loops were formed by the accumulation of interstitials. At intermediate temperatures, impurities play an important role for the nucleation of loops. At higher temperatures, interstitials are de-trapped from impurities and the effect of the impurity is not dominant. These tendencies are clearly shown in the figure.

4.2. Proton and helium ion irradiation

Irradiation experiments for five kinds of tungsten were carried out at 80 °C using a He ion beam of about 1 μA with 3.0 MeV and a proton beam with 850 keV accelerated by Dynamitron accelerator in Tohoku University. To measure the swelling of the irradiated area, a 25 μm lattice copper mesh (10 μm in thickness) was fixed on the irradiated surface, which created an irradiated region and unirradiated region simultaneously. The projected range of implanted ions in a W was about 4.5 μm. In order to obtain a region with a uniform gas atom distribution in the implanted area, an energy degrader was used during the irradiation. The calculated irradiation dose are: (a) He 2000 appm (0.077 dpa) and 4000 appm (0.154 dpa), (b) He 2000 appm before H 20 000 appm and (c) H 20 000 appm (0.04 dpa).

The following results were obtained:

(1) The surface morphology change using a surface profiler showed a step height of about 30 μm only in the CVD-W, which was implanted 20 000 appm H after 2000 appm He implantation.
(2) Irradiation hardening was observed in all the irradiated specimens. The magnitudes of the hardening caused by He-ion implantation showed almost the same trend for all samples, as shown in Fig. 18.
(3) The effect of the existence of implanted He on the irradiation hardening was larger than that of H. This was probably because the displacement damage played a major role in the hardening under this experimental condition.

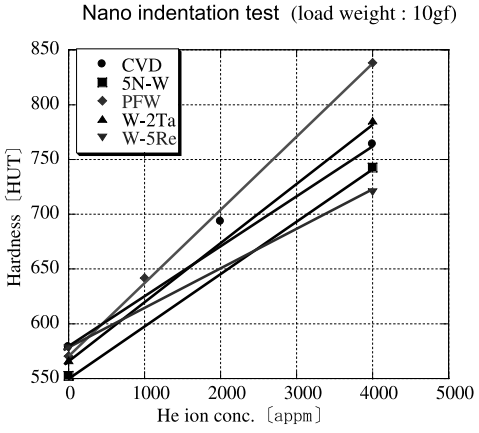

Fig. 18. Hardness change of irradiated tungsten with the implanted helium concentration.

5. Calculations of thermal-hydraulics and neutronics performance of a solid tungsten target

5.1. Thermal-hydraulics calculations

Thermal-hydraulic designs for an intense pulsed neutron source with a solid target composed of tungsten were made to determine the material and the shapes of the target and its vessel to cool them safely and to obtain a high-neutron flux.

Attention should be paid to the thermal-hydraulic designs to cool the target safely under the following conditions:

(1) The coolant conduit is designed to obtain a uniform and stable flow.
(2) The heat flux at the target surface should be below the critical heat flux.
(3) The temperature at the target surface should be below the saturation temperature of the coolant water to avoid boiling inception. In the present work, the wall temperature was kept below 120 °C.
(4) The thermal stress in the target should be below a certain value smaller than the yield stress or the stress which causes a deformation of the coolant channel.
(5) The coolant water fraction of the target should be as small as possible by optimizing the gap between the tungstens, to obtain a high-density target.
(6) The after heat should be low enough when the target is changed.

Fig. 19 shows the solid target model: (a) the slab type target model, the length of the plate: 167 mm, width: 60 mm and (b) the rod type model, with parallel coolant flow. Tungsten was clad by tantalum for slab type and inserted into tantalum or a Zircaloy sheath of 0.5 mm thickness for the rod type. Rods were separated from each other by wrapping wires. The gap between the rod and the sheath was 50 μm and filled with helium gas. The coolant velocity was10 m/s, and the pressure was 1 MPa. Temperature of inlet coolant was 30 °C. Slab thickness and rod diameter were determined considering the criterion through (1)–(6). The maximum temperature was set below 200 °C, giving maximum thermal stress of 100–200 MPa.

The power density in the solid was calculated by the Monte Carlo method by Kiyanagi and co- workers [21]. The resultant power density profile along the center axis of the solid target with a proton beam power of 1 MW is given by

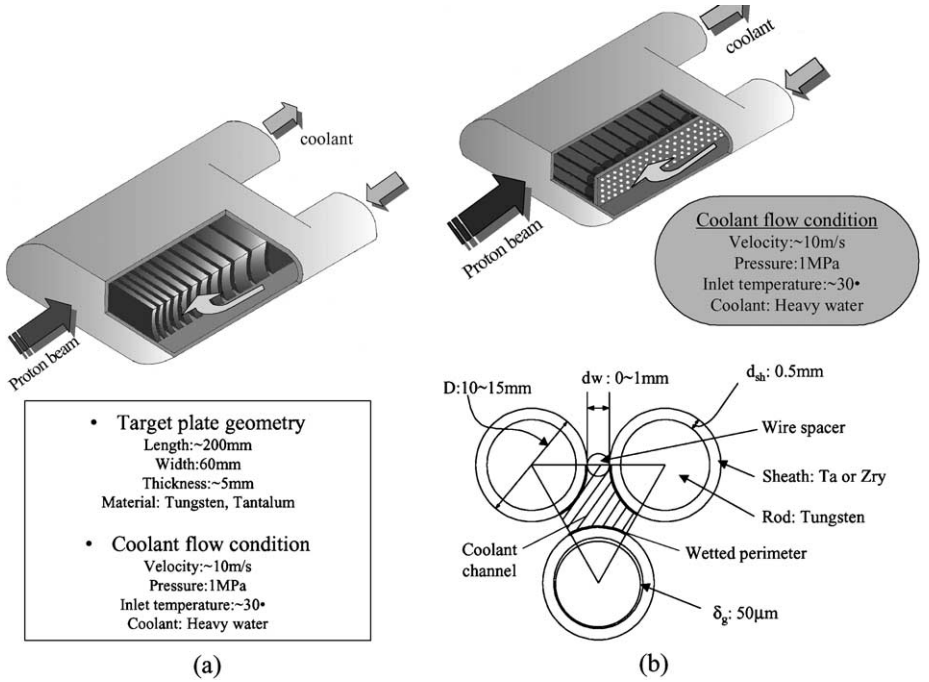

Fig. 19. Solid target model. (a) Plate type target, (b) rod array target cooled by parallel flow.

$$Q(z) = 1600[1 - \exp\{-(z + 1.9)/4.7\}] \times \exp(-z/1.16)\ (\mathrm{MW/m^3}), \quad (2)$$

where z is the distance from the front of the target.

A stress analysis of a rod with both ends free was performed. In the case of the operating condition at 1 MW, the temperature was distributed from 1000 to 950 °C in the center of the tungsten rod and from 140 to 80 °C in Zircaloy sheath. The thermal stress to tungsten was 52 MPa (tension) at the surface and 65 MPa (compression) at the center axis, which indicates that the rod array target was feasible in view of thermal stress as well as thermal-hydraulics. The temperature difference of 60 °C in the sheath gave a thermal stress of about 40 MPa tension and compression. These values are permissible for Zircaloy.

The neutron flux at the exit of the moderator was roughly proportional to the target averaged density in the effective target area for the moderators. Fig. 20 compares the average density of a tungsten plate target

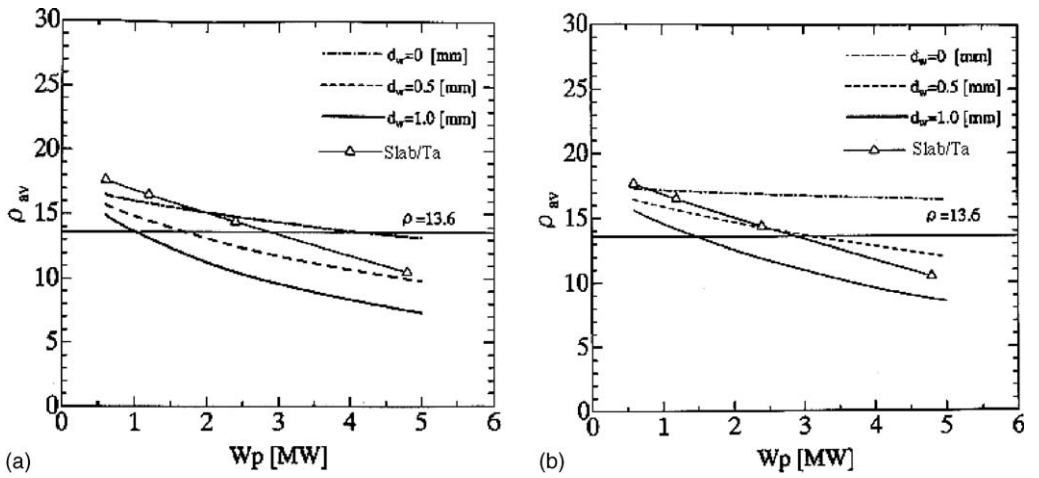

Fig. 20. Comparison of the average densities of a solid target with mercury. (a) Zircaloy sheath, (b) Ta sheath.

and tungsten rod targets sheathed by Zircaloy or tantalum as a function of the beam power up to 5 MW with the mercury density; d_w is a diameter of the wrapping wire. The average density of slab target clad by tantalum was larger than the mercury density below about 3 MW. As for a rod target of $d_w = 0.5$ mm, the average density was larger below 1.5 MW for the Zircaloy sheath and 3 MW for the tantalum sheath.

5.2. Calculation of the neutronic performance of a solid tungsten target

The neutronic performance was investigated by Monte Carlo calculations using the MCNPX code [22]. The TMRA (target-moderator-reflector assembly) was modeled based on a model of that of Japanese spallation neutron source (JSNS) in the JAERI-KEK High Intensity Proton Accelerator Project [23]. A mercury target was bombarded by a pulsed proton beam of 3 GeV and 333 μA with repeat rates of 25 Hz. Three kinds of solid targets were calculated: (1) 0.5 mm-tantalum clad tungsten with slab geometry and (2), (3) tungsten rod in Zircaloy or tungsten sheath of 0.5 mm thickness. The models of the targets were based on the geometry that were determined in the thermal-hydraulic designs described in the preceding subsection. As for slab target, target thickness was taken from 6.25 mm at the front side to 37.5 mm at the back side, and the gap between the slabs was 1.5 mm. The separation of the rod target, i.e., the diameter of the wrapping wire, d_w, was taken as 0, 0.5 and 1 mm. The rod diameters were 12.1 mm, in the case of Ta sheath and $d_w = 1$–15.3 mm in the case of Zircaloy sheath and $d_w = 0$ mm. The moderator was composed of 100% para-liquid hydrogen. The decoupler that reshaped a neutron pulse sharp was new one composed of 81% silver and 14% indium, 5% cadmium in atom density and gave a decoupling energy of 2 eV. Fig. 21 shows the moderator configuration. A coupled moderator was set upon the target. Decoupled and poisoned moderators were placed below the target. The reflector was lead in which there were considered various casks, structure materials and cooling channels according to a realistic model used for the actual designs. The beam distribution was uniform distribution with 13 and 5 cm. In the case of a solid target, the target height and width were optimized to attain the highest neutron fluxes from the moderators. Heavy water was used as a coolant of the target. The calculated results are given below.

The optimum target size of plate type one was determined to be 7 cm height × 19 cm width; the D_2O plenum width was 4 cm. The neutron energy-integrated intensities are given by the ratio to those of the mercury target in Table 1. The values as a function of neutron energy are nearly constant: 1.09 for the coupled moderator, 0.99–1.04 for the decoupled moderator and 1.05 for the poinsoned moderator.

Table 2 shows the ratio of the neutron intensities in the case of the rod type with a tantalum sheath for

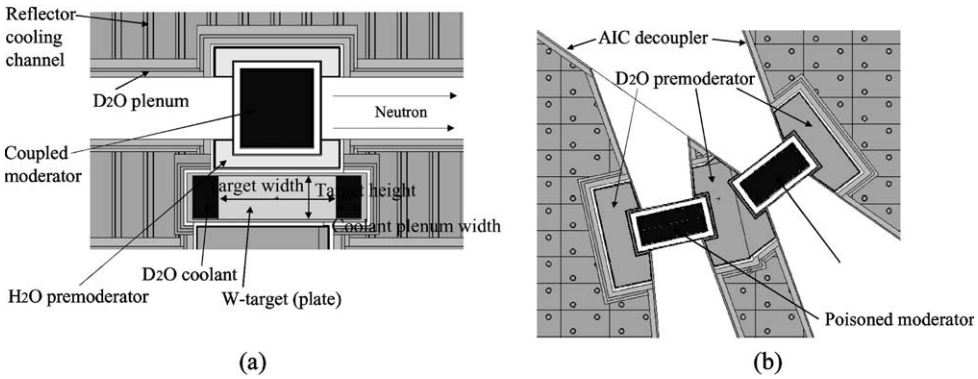

Fig. 21. Moderator configuration reflected with lead. (a) Side view, (b) plane view.

Table 1
Ratio of the neutron intensities in the case of a slab target

Energy range (meV)	Ratio of integrated neutron intensity to that of mercury target		
	Coupled moderator	Decoupled moderator	Poisoned moderator
0–5	1.09	1.04	1.05
5–25	1.09	1.02	1.05
25–100	1.09	1.02	1.05
100–500	1.09	0.99	1.05

Table 2
Ratio of the neutron intensities in the case of the rod type with a tantalum sheath

Moderator		$d_w = 0.1$ mm	$d_w = 0.5$ mm	$d_w = 0.0$ mm
	Ratio of density	1.07	1.17	1.26
	Energy interval (meV)	Ratio of integrated neutron intensity to that of mercury target		
Coupled moderator	0–5	0.97	1.03	1.09
	5–25	0.97	1.03	1.08
	25–100	0.98	1.04	1.09
	100–500	0.98	1.06	1.10
Decoupled moderator	0–5	0.94	0.97	1.00
	5–25	0.94	0.97	0.99
	25–100	0.93	0.97	0.98
	100–500	0.94	0.98	0.99
Poisoned moderator	0–5	0.93	1.02	1.06
	5–25	0.94	1.03	1.08
	25–100	0.95	1.04	1.08
	100–500	0.91	1.02	1.03

individual wrapping wire diameters. The ratio values for $d_w = 0.5$ mm, that is the frequently adopted in nuclear reactors, were 1.03–1.06 for the coupled moderator, 0.97–0.98 for the decoupled moderator and 1.02–1.04 for the poisoned moderator. In the case of the Zircaloy sheath, the values were smaller by about 2% than for the tantalum sheath. This means that the solid target at 1 MW had almost the same neutron performance compare to that of the mercury target. The values are smaller than the average target density ratio to some extent.

Fig. 22 shows the neutron pulse from the poisoned moderator. At En = 12 meV, the pulse peak of the solid targets are obviously higher than that of the mercury target. The logarithmic graph on the left hand side shows that the pulse decay shapes are very similar to each other, except for that after 100 ms, where the neutron fluxes fluctuate because of worse statistical errors. Thus, a better or similar performance of the neutron pulse is excepted to a solid target compared to a mercury target.

6. Conclusion

Efforts to develop a solid target have been made for MW-class spallation neutron sources A tungsten target is the most promising because of its high-neutron yield and high toughness at high temperature. However, it has a disadvantage of low corrosion resistance to water under the condition of high temperature and radiation.

In order to overcome the weak points, we investigated the applicability of three cladding techniques with tantalum. The HIP method was established: optimum

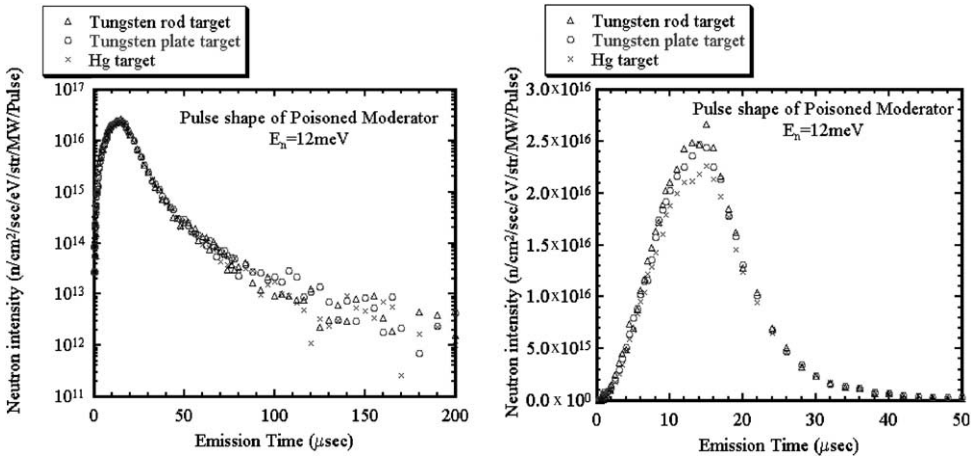

Fig. 22. Neutron pulse shape from a poisoned moderator.

Table 3
Score of target materials for a MW-class spallation neutron source

Requirement	Bare W	Bare Ta	Bare Zr-2	Clad W	Clad U	Clad Pb
Net neutron yield	4	3	1	3.5[a]	5	3
Operating experience	3	5	5	4	4	1
Development issues	4	4	5	4.5[a]	2	1
Compatibility issues	3[a]	4	4	3	3	3
Radiation damage issues	3[a]	4	4	4	1	1
Post-irradiation issues	1	2	2	1	1	2
Radiation hazard[a]	3[a]	1[a]	4[a]	3[a]	0[a]	4[a]
Target size[a]	4[a]	4[a]	2[a]	4[a]	4[a]	3[a]
Total/Product	25/5184	27/7680	27/6400	27/9072	20/0	18/216
Rank	4	2	3	1	6	5

[a] Changed from the Powel's evaluation [24].

HIP'ing condition was found and verified by testing the specimen with the SP method. The key of a successful HIP is to control the environment condition during HIP'ing by using high-purity argon gas and impurity-gas getters. It is also important to fabricate both the tungsten block and tantalum case with a high fabrication accuracy, and not to harden the tantalum components by suitably annealing fabricated tantalum components. Especially, fine fabrication of a straight hole in the tungsten block is important, as a crack of tantalum sheath [8] inserted into the hole of tungsten block was likely due to crude fabrication of the hole. Finally, it was well applied to an actual target for KENS. However, KENS is only 3 kW, and it is necessary to investigate if the tantalum clad tungsten target processed by the HIP method will be well used enough times for a MW-class source. A neutron scattering analysis of the HIP'ed specimen will be interesting to analyze the stress stored through the fabrication and HIP'ing. It was also found that brazing and electrolytic coating techniques are essentially applicable. Further investigation is needed for seeking the optimum conditions to realize them in the sense of engineering. The development of a new material, such as heavy metal including stainless steel to increase resistance to corrosion, was tried and metallurgy process was built-in, although the produced material contained some chemical compounds that lost a good property of tungsten alloy processed by liquid-phase sintering. Further investigations are needed to produce a desirable material.

A corrosion test of various tungsten and tungsten alloys in water with a low flow-rate shows that pure tungsten is hardly corroded by water, and a bare tungsten target may be used. However, the test with a high flow-rate denied such a bare target because tungsten was remarkably corroded by fast water flow. Accordingly, clad is indispensable.

There are few data of radiation damage for tungsten, except for some experiments for fusion rectors and the LANSCE target. The PIE data of several specimens of tungsten irradiated at the SINQ target will be very useful for evaluating the lifetime of a target. Trials of irradiation by electrons, protons, and helium ions have been made and basic data were obtained to understand the mechanism of radiation damage.

Thermal-hydraulic and neutronic designs clarified that a solid target will be available for a MW-class spallation neutron source. Its neutron performance at 1 MW is very similar or superior to that of a mercury target, though optimization of TMRA configuration was not made sufficiently compared to a mercury target which was used as a reference in the present work. It should be noted that most engineering techniques of rod-type target using a Zircaloy sheath have been established in the field of nuclear reactors. A tantalum clad target will also be promising if the reliability of a tungsten–tantalum bond will be confirmed.

Recently, Powel [24] evaluated candidates of materials used for a solid target back-up for the SNS, and summarized his evaluated result in the table. We reevaluated it, while considering the results of our work and the experiences of using a tungsten target at LANSCE [11,12] that rod-type tungsten block could be used sufficiently without any break up to a dose rate of about 25 dpa as well as nuclear hazards of fission products and induced activities. Table 3 shows our evaluation. The total score shows that the highest value (27) can be seen in the field of bare Ta, bare Zircaloy-2 and clad W. As for clad U, a radiation hazard due to fission products is essentially of a problem, and is as severely controlled as nuclear plants. Therefore, zero score is given to reject it. We ranked the target materials according to the product of the scores. The first candidate is presently clad tungsten.

Acknowledgements

This work was performed with Support by a Grant-in-Aid for Scientific Research from Monbu-Kagaku-sho (Ministry of Education, Culture, Sports, Science and Technology) during April 1999 to March 2002. The

authors are highly indebted to Dr Manabu Satoh of Tohoku University for cooperative works on irradiation experiments, and to Dr Yasuhiro Ishijima of Tohku University, and Dr Kazuo Kakiuchi and Dr Takemi Furuya of Nuclear Fuel Industries on corrosion tests. They would gratefully appreciate to Mr Kenichi Okamoto and Mr Masahiro Katoh of A.L.M.T. Corp. for their assistance on preparing the specimens of corrosion tests and components of target block for study on HIP, to Mr Yasu Manabe of Kobe Steel Ltd. for their helpful works on the HIP process and to Mr Toru Miyata of Hitachi Kenki Fine Tech. Co. Ltd. for their kind cooperation to make an ultrasonic diagnostic of the HIP'ed block using their instruments.

References

[1] Y. Ishikawa, Proceedings of the Fourth Meet. of the International Collaboration on Advanced Neutron Sources (ICANS-IV), KEK, Tsukuba, 20–24 October 1980, KEK, March 1981, p. 181.
[2] G. Russel, H. Robinson, G.L. Legate, R. Woods, E.R. Whitaker, A. Bridge, K.J. Hughes, R.D. Neef, Proceedings of the ICANS-IX, Villigen, 22–26 September 1986, SIN Villigen, July 1987, p. 177.
[3] M.W. Cappiello, A.M. Baxter, in: Proceedings of the Second International Topical Meeting on Nuclear Applications of Accelerator Technology, Gatlinburg, Tennessee, 20–23 September 1998, ANS, 1998, p. 289.
[4] T. Kawamura, Sumitomo Technical Report 3-146, 1995, p. 78.
[5] H. Ullmaier, F. Carusughi, Nucl. Instr. and Meth. B1-1 (1995) 406.
[6] Y. Kitsunai, H. Kurishita, H. Kayano, Y. Hiraoka, T. Igarashi, T. Takida, J. Nucl. Mater. TiC 271&272 (1999) 423.
[7] M. Kawai, K. Kikuchi, H. Kurishita, J. Li, M. Furusaka, J. Nucl. Mater. 296 (2001) 312.
[8] M. Kawai, S. Yasui, M. Furusaka, T. Ino, N. Torikai, Y. Kiyanagi, Proceedings of the 15th Meeting, International Collaboration on Advanced Neutron Sources, ICANS-XV, 6–9 November 2000, Tsukuba, KEK Proceedings 2000-22, vol. II, 2001, p. 747.
[9] Y. Dai, G.S. Bauer, J. Nucl. Mater. 296 (2001) 43.
[10] J. Chen, T. Flossdorf, F. Carusughi, T. Broome, H. Ullmaier, Programme/Abstacts of Fourth International Workshop on Spallation Material Technology, 8–13 October 2000, Schruns, Austria, Paul Scherrer Institute, p. 38.
[11] P. Ferguson, private communication, 2001.
[12] S.A. Maloy, M.R. James, W. Sommer Jr., G.J. Willcutt Jr., M. Lopez, T.J. Romero, Mater. Trans. 43 (4) (2002) 1.
[13] T. Broome, Proceedings of Second International Workshop on Spallation Materials Technology, Ancona, Italy, 19–22 September 1997, jul-3450, p. 55.
[14] M. Saito, H. Takahashi, H.D. Jeong, A. Kawasaki, R. Watanabe, Trans. JSME 57 (1991) 522.
[15] R. Watanabe, A. Kawasaki, M. Tanaka, J.-F. Li, Int. J. Refract. Metals Hard Mater. 12 (1993–1994) 187.
[16] R. Watanabe, J.-F. Li, A. Saito, H. Kurishita, T. Igarashi, K. Okamoto, K. Kikuchi, M. Furusaka, M. Kawai, Proceedings of the 15th International Plansee Seminar 2001, May 28–June 1 2001, Reutte, Austria, vol. 4, p. 1.
[17] S. Shimodaira, Material Science of Corrosion and its Protection, 2nd Edn., AGNE, 1995.
[18] L.L. Shreir, R.A. Jarman, G.T. Burstein (Eds.), Corrosion, vol. 1, 3rd Ed., Butterworth-Heinemam, 1994.
[19] Y. Ishijima, K. Kakiuchi, T. Furuya, H. Kurishita, M. Hasegawa, T. Igarashi, M. Kawai, J. Nucl. Mater. 307–311 (2002) 1369.
[20] H.H. Uhlig (Ed.), Corrosion Handbook, Wiley, 1948.
[21] N. Hata, K. Kitazaki, Y. Kiyanagi, Proceedings of the International Workshop on JHF Science, 3–7 March 1998, KEK Proceedings 98-5, vol. III, p. 8; Y. Kiyanagi, private communication.
[22] H.G. Hughes, R.E. Orael, R.C. Little, MCNP-X – The LAHET/MCNP Code Merger, LA-UR-97-4891, Los Alamos National Laboratory, 1997.
[23] The Joint Project Team of JAERI and KEK, The Joint Project for High-Intensity Proton Accelerators, KEK Report 99-4, 1999.
[24] S.J. Powel, Preliminary Materials Recommendation for a Solid Target Back-Up for the SNS, SNS/T SR-0149, 1999.